

Article

# Robust Stabilization of a Microgrid with Communication Delay and Uncertainties

Ashraf Khalil <sup>1,\*</sup> , Asma Alfergani <sup>2</sup>, Farhat M. Shaltami <sup>3</sup> and Ali Asheibi <sup>4</sup><sup>1</sup> DTU Engineering Technology, Technical University of Denmark, 2750 Ballerup, Denmark<sup>2</sup> Electrical and Electronics Engineering Department, University of Benghazi, Benghazi 3332, Libya<sup>3</sup> Electronics and Communication Technology Department, College of Electrical and Electronics Technology—Benghazi, Benghazi 16063, Libya<sup>4</sup> Department of Electronics and Communications Engineering, College of Engineering, A'sharqiyah University, Ibra 400, Oman

\* Correspondence: ashka@dtu.dk

**Abstract:** In this paper, the robust stabilization for the networked microgrid system is presented. A microgrid implements master-slave control architecture where the communication channel is utilized to exchange the reference current signals. With this structure, a time delay exists in the reference control signal which may lead to instability. The analysis of the control strategy is carried out in dq reference frame. The microgrid is constituted by PV and wind energy sources supplying a load through voltage source inverters. The stochastic nature of renewable energy sources introduces uncertainties which can be represented as fluctuations in the voltage and the current. The main contribution of the paper is formulating the controller design of the microgrid with communication delay and uncertainties in the model as  $H_\infty$  control problem and Lyapunov–Krasovskii functional is utilized to develop stability criterion in bilinear matrix inequality form. Grey wolf optimizer is used to minimize the performance index and derive the stabilizing controller. The microgrid performance is tested through simulation using the time-varying nonlinear model of the microgrid. The results prove that satisfactory current and power-sharing are attained even with the existence of time delays and uncertainties.



**Citation:** Khalil, A.; Alfergani, A.; Shaltami, F.M.; Asheibi, A. Robust Stabilization of a Microgrid with Communication Delay and Uncertainties. *Computation* **2023**, *11*, 75. <https://doi.org/10.3390/computation11040075>

Academic Editors: Ali Cemal Benim and Markus Kraft

Received: 19 December 2022

Revised: 25 March 2023

Accepted: 3 April 2023

Published: 7 April 2023



**Copyright:** © 2023 by the authors. Licensee MDPI, Basel, Switzerland. This article is an open access article distributed under the terms and conditions of the Creative Commons Attribution (CC BY) license (<https://creativecommons.org/licenses/by/4.0/>).

**Keywords:** AC microgrid; communication delay; GWO;  $H_\infty$ ; Lyapunov–Krasovskii; control strategy; parallel inverter; robust stability; SVPWM; uncertainty

## 1. Introduction

Sustainable energy is a promising solution for major challenges such as global warming, increasing demands for energy, and insufficiency of fossil fuel. Sustainable power systems are constructed of renewable energy sources, which include microturbines, photovoltaic (PV) panels, wind farms, fuel cells, combining heat and power units, etc., see Figure 1. To make full use of the renewable energies and build a sustainable power system, distributed generation (DG) is implemented. Because DG generates power near the consumers, the transmission line losses are reduced and the need for expanding the power system infrastructure will be avoided. However, the power generated from renewable energy is uncertain. This uncertainty may affect the stability of the grid. The idea of Microgrid is being studied and developed by many researchers to eliminate the disadvantages of DGs. Microgrid is a unique entity which is constructed from DGs, storage units, coordinated by a control system through communication channel. Communication system is responsible for the communication between microgrid and the energy management system, in case of communication-based control strategy of the MG [1–3]. The control of the microgrid remains one of the utmost challenges facing widespread application. Master-slave control strategy has attracted many researchers because of the distribution of the control tasks among the units. Moreover, the single point of failure can be eliminated. Besides that, the

current sharing is improved with proper controller design. In this paper, the master-slave control scheme is implemented. This control strategy is implemented by assigning one of the inverters as a master inverter and the other inverters as slaves. A communication network is used in this strategy which creates a networked distributed system [4]. The microgrid under study consists of PV array connected to the bus through DC-DC converter and an inverter, and a wind turbine with a permanent synchronous generator connected to the bus through a rectifier and an inverter. This system has been investigated in [4–10]; however, the impacts of the uncertainties in the renewable energy generation has not been taken into account. The time delay present in the control loop in addition to the uncertainty brings many challenges to the controller design. In the next section we review some of the results published in the literature.

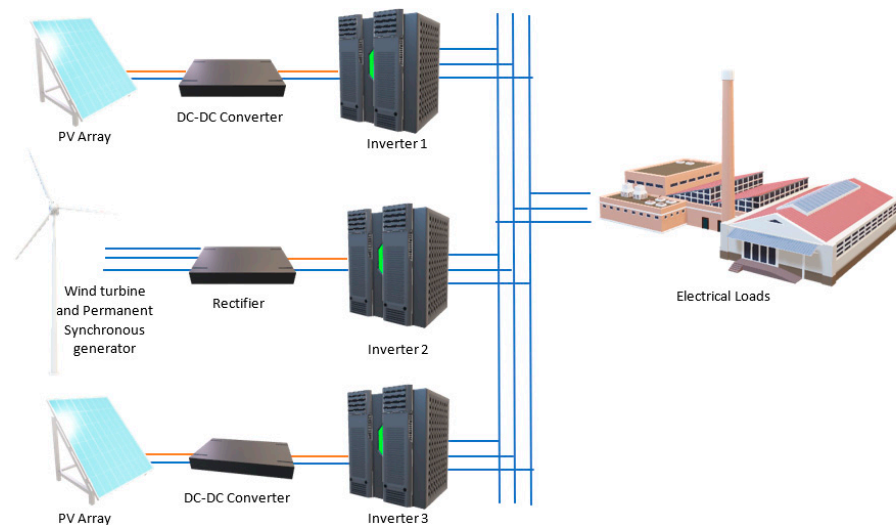


**Figure 1.** A hybrid microgrid with  $n$ -parallel inverters.

Authors in [11] used a broadcast gossip algorithm in their proposed control scheme to guarantee the average value of the voltage generated from distributed energy sources to be regular. Authors in [12,13] considered communication delays and slow switching topologies in their proposals. In [12], a dual agent distributed cooperative method aimed at a dc MG to assure a voltage regulation was proposed. In [13], a distributed cooperative control strategy for dc microgrid is proposed. Authors in [14] used extreme learning machine (ELM) algorithm to get precise power compensation under abnormal communication delay (ACD). To regulate the voltage and the power of microgrid instantaneously, authors in [15] synthesized a multiagent controller while wireless communication is used between parallel inverters. To eliminate the adverse effects of delays, authors in [16] determined the time delays by implementing a controller based on a sliding mode estimation. Authors in [17] used the solution of delayed differential equations to compute the allowable delay for distributed secondary control algorithm. Authors in [18] implement a control strategy based on distributed iterative event triggered for microgrid to reduce the communication. Authors in [19] designed a consensus-based secondary control to handle the communication interruption problem (CIP) in the secondary control process of DERs using the path reconstruction method. In [20], a strategy for triggering to overcome the delay in the communication network is designed. To limit the communication delay impacts on the system, the authors in [21] presented a control scheme for frequency restoration in islanded AC microgrid. To improve the stability of the microgrid the virtual synchronous generator method is implemented in [22]. Like in [19], event-triggered communication in [22] reduces the communication resources.

In [23,24], active power sharing is the main objective using consensus-based distributed control. Both methods are robust to system parameter variations. However, they both have limitations regarding communication delays and packets losses. Research

in [25–32] dealt with the time varying delay using  $H_\infty$  robust control theory. In [25], the sliding-mode control and mixed  $H_2/H_\infty$  optimal control are used to stabilize the microgrid with uncertainties. The multi-agent approach is presented in [26], where  $H_\infty$  is implemented. In [27],  $H_\infty$  and  $\mu$  synthesis are used to achieve the robustness of the frequency in an islanding microgrid. In [28], a delay-dependent robust stability-based  $H_\infty$  is used to improve the voltage performance. The virtual inertia with PLL is implemented in [29]. An  $H_\infty$  is compared with the conventional and optimal PI virtual inertia control, and it is reported that performance of the  $H_\infty$  is superior. In [30], the robust virtual inertia control with a coefficient diagram method is applied to islanding microgrid. The resilience  $H_\infty$  is applied in [31]. The robustness of these techniques to delays and packets losses is enhanced. In addition, these techniques are robust to system parameters variations. Research in [33–35] consider constant delay where adaptive neural predictive control is used to increase the robustness against communication delays and system parameters variations. In [36–41], synchronization control is used for constant delay, where the robustness of the systems to delay and packet losses is improved.

The focus of the paper is the robust stability of microgrid with variable time delay and uncertainty affected by the renewable energy sources. The variable time delay makes it challenging to analyze and design the microgrid. The main contribution of the paper is formulating the controller design problem as  $H_\infty$  problem, and applying Lyapunov–Krasovskii functional (LKF) then a stability criterion is developed in the form of bilinear matrix inequality (BMI). There are many intelligent optimization techniques that can be utilized to solve such a problem. The grey wolf optimization (GWO) is implemented to solve the BMIs and minimize the performance index. The paper is organized as follows: Section 2 describes in detail the dynamic model of PV/wind microgrid. Section 3 introduces the master-slave control strategy in the  $dq$  reference frame while Section 4 introduces the robust controller design procedure along with solving the BMIs with the aid of GWO. In Section 6, the proposed method is applied to two-inverters microgrid, and the performance of the controller is proved using simulation where the nonlinear models of the inverters are used.

## 2. The Dynamic Model of the Microgrid

The microgrid is based on renewable energy sources and power electronic converters, where their models are nonlinear and time-varying system, and their analysis requires advanced level of mathematics. The time average model of the microgrid is shown in Figure 2. The analysis is carried out in the  $dq$  reference frame where the current and voltage variables are transformed from  $abc$  rotating frame to  $dq$  reference frame using Park’s transformation. According to [4,9], the states of the microgrid are described by the linearized model as:

$$\dot{x} = Ax(t) + Bu(t) \tag{1}$$

where the states of the microgrid variables are augmented as  $x$ , the duty cycles are  $d$ , the control input,  $u$ ,  $w(t)$  is the exogenous disturbance, these vectors are given as:

$$x = [v_d \ v_q \ i_{d1} \ i_{q1} \ i_{d2} \ i_{q2} \ V_d \ V_q \ I_{d1} \ I_{q1} \ I_{d2} \ I_{q2}]^T$$

$$u = [d_{d1} \ d_{q1} \ d_{d2} \ d_{q2}]^T, \ w(t) = [w_1(t) \ w_2(t)]^T$$

$A, B$  are constructed as [4]:

$$A = \begin{bmatrix} A_{11} & A_{12} \\ A_{21} & A_{22} \end{bmatrix}$$



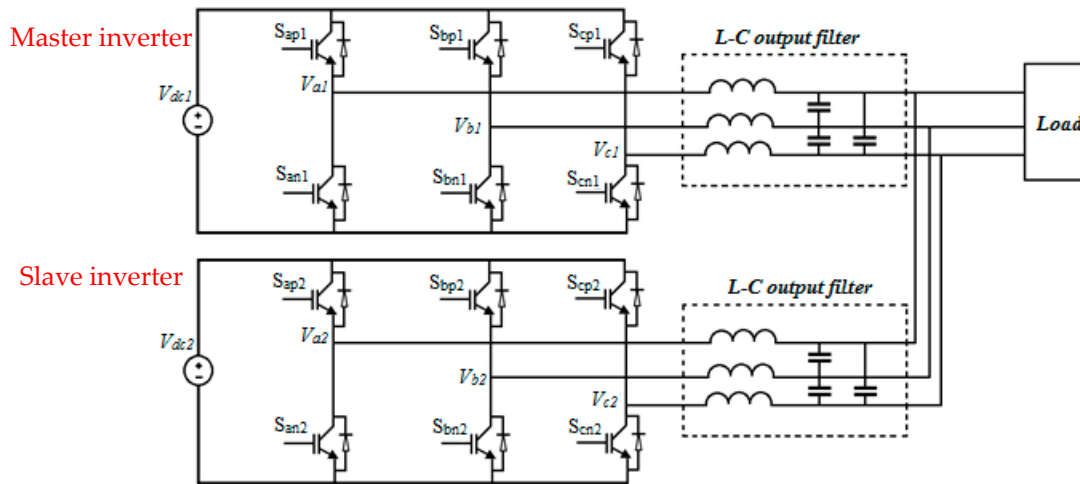


Figure 2. The dynamic model of the two parallel inverters.

The parameters in matrices *A* and *B* are given in Table 1.

Table 1. The parameters of the microgrid.

The Paramter	Definition
$i_{d1}$ and $i_{d2}$	The direct component of the current of the first and the second inverter
$i_{q1}$ and $i_{q2}$	The quadrature component of the current of the first and the second inverter
$C$	The capacitor in the filter
$L_1$ and $L_2$	The inductances of the filters
$R$	The load resistance
$v_d$ and $v_q$	The direct component and quadrature component of the output voltage
$I_{d1}, I_{d2}, I_{q1}, I_{q2}, V_d,$ and $V_q$	The filtered currents and voltages
$\omega$	The radian frequency of the system
$D$	The duty ratio

It should be noted that  $V_{dc1}$  is the output voltage of the step-up DC/DC converter and  $V_{dc2}$  is the output voltage of the rectifier. The model of the PV panel is given as [10]:

$$I(T, G, V) = \left( G/G_{nom} I_{ph0} \right) - (V + I \cdot R_s) / R_{sh} - \left( \left[ \exp(-E_g / V_s (1/T - 1/T_1)) \right] \left( T/T_1 \right)^{3/n} I_{SC(T_1)} \right] \left( e^{(V + IR_s) / nV_{th}} - 1 \right) \tag{2}$$

$$I(T, G, V) = I_{ph} - I_{sh} - I_D \tag{3}$$

The parameters in (2) and (3) are defined according to [42];

$$I_{ph}(T) = I_{ph} + \left( [1 / (T_2 - T_1)] \right) \left( I_{ph}(T_2) - I_{ph}(T_1) \right) (T - T_{meas}) \tag{4}$$

$$I_0(T_1) = I_{SC(T_1)} / \left( \exp(qV_{OC(T_1)} / nkT_1) - 1 \right) \tag{5}$$

$$R_s(T) = -1 / (I_0(T_1) \cdot q / nkT_1 \cdot e^{qV_{OC(T_1)} / nkT_1}) - dV / dI_{V_{OC}} \tag{6}$$

$$R_{sh} = V_{OC} / \left( I_{ph} - I_0 \left[ \exp(qV_{OC} / nkT_{meas}) - 1 \right] \right) \tag{7}$$

$$R_{sh}(T) = (T / T_{meas})^\alpha R_{sh} \tag{8}$$

The parameters of the PV array are given in [10]. The model described by (2)–(8) is implemented in Matlab/Simulink (2018b) where the PV source consists of 210 PV solar panels. The PV array is arranged to have ten parallel branches, and each has 22 PV panels connected in series [10]. The IV characteristics of the PV panel are given in [10]. The mechanical power of the wind turbine is given by [43]:

$$P_m = 0.5\rho a C_p v_w^3, \text{ with } \lambda = \omega R / v_w \tag{9}$$

where  $\rho$  is the density of air (Kg/m<sup>3</sup>),  $a$  is the area of the turbine blades (m<sup>2</sup>),  $R$  is the radius of the blades,  $v_w$  is the wind speed (m/s),  $\omega$  is the rotational speed of the turbine blades (rad/s). The power coefficient  $C_p$  is given as [43]:

$$C_p(\lambda) = c_1 \left( \frac{c_2}{\lambda} - c_4 \right) e^{-c_5/\lambda} + c_6 \lambda \tag{10}$$

where  $\beta$  is the pitch angle and  $\lambda$  is the tip speed. For this turbine, the maximum output power is reached with  $\lambda = 8.1$  and  $C_p = 0.48$ . The constants are given as:  $c_6 = 0.0068$ ,  $c_4 = 5$ ,  $c_3 = 0.4$ ,  $c_2 = 116$ ,  $c_2 = 116$ ,  $c_1 = 0.5176$  [43]. The wind turbine rated power and rated speed are 20 kW and 12 m/s respectively. The cut-in speed of the turbine is 5 m/s and the cut-out speed is 25 m/s, the radius of the blade is 5 m [43]. The permanent synchronous generator is four poles machines and the inertia constant is 0.08 kg.m<sup>2</sup>, the dynamic model parameters are:  $L_d = L_q = 0.95$  mH, the stator windings equivalent resistance is 0.085  $\Omega$ , and the viscosity damping is 0.001147 N. m. s [44]. For more details on the PV array and wind turbine model, the reader can refer to [4].

### 3. The Closed Loop Model with Uncertainty and Time Delay

The control tasks are divided between different controllers where the voltage is regulated by the master, Figure 3. Both the master and the slave unit have current controllers but the current sharing signal is produced by the master controller [4]. The reference currents are distributed by the master controller to all the slave units through a kind of communications network. The reference current signals experience time delay and data loss. The model of the controllers is given by [4]:

$$\dot{z} = Ex(t) + Fz(t) + E_d x(t - \tau) + F_d z(t - \tau) + B_d w(t) \tag{11}$$

$$u = u(t) + u(t - \tau) \tag{12}$$

$$u = Cx(t) + C_d x(t - \tau) + Dz(t) + D_d z(t - \tau) \tag{13}$$

where

$$z = [\Phi_d \quad \Phi_q \quad \gamma_1 \quad \gamma_2 \quad \gamma_3 \quad \gamma_4]^T$$

$$E = \begin{bmatrix} 0 & 0 & 0 & 0 & 0 & 0 & -1 & 0 & 0 & 0 & 0 & 0 \\ 0 & 0 & 0 & 0 & 0 & 0 & 0 & -1 & 0 & 0 & 0 & 0 \\ 0 & 0 & 0 & 0 & 0 & 0 & 0 - K_{vdp} & 0 & -1 & 0 & 0 & 0 \\ 0 & 0 & 0 & 0 & 0 & 0 & 0 & -K_{vqp} & 0 & -1 & 0 & 0 \\ 0 & 0 & 0 & 0 & 0 & 0 & 0 & 0 & 0 & 0 & -1 & 0 \\ 0 & 0 & 0 & 0 & 0 & 0 & 0 & 0 & 0 & 0 & 0 & -1 \end{bmatrix}$$

$$E_d = \begin{bmatrix} 0 & 0 & 0 & 0 & 0 & 0 & 0 & 0 & 0 & 0 & 0 & 0 \\ 0 & 0 & 0 & 0 & 0 & 0 & 0 & 0 & 0 & 0 & 0 & 0 \\ 0 & 0 & 0 & 0 & 0 & 0 & 0 & 0 & 0 & 0 & 0 & 0 \\ 0 & 0 & 0 & 0 & 0 & 0 & 0 & 0 & 0 & 0 & 0 & 0 \\ 0 & 0 & 0 & 0 & 0 & 0 & 0 - K_{vdp} & 0 & 0 & 0 & 0 & 0 \\ 0 & 0 & 0 & 0 & 0 & 0 & 0 & -K_{vqp} & 0 & 0 & 0 & 0 \end{bmatrix}$$

$$\begin{aligned}
 C_d &= \begin{bmatrix} 0 & 0 & 0 & 0 & 0 & 0 & 0 & 0 & 0 & 0 & 0 & 0 \\ 0 & 0 & 0 & 0 & 0 & 0 & 0 & 0 & 0 & 0 & 0 & 0 \\ 0 & 0 & 0 & 0 & 0 & 0 & -K_{idp2}K_{vdp} & 0 & 0 & 0 & 0 & 0 \\ 0 & 0 & 0 & 0 & 0 & 0 & 0 & -K_{iqp2}K_{vqp} & 0 & 0 & 0 & 0 \end{bmatrix} \\
 D_d &= \begin{bmatrix} 0 & 0 & 0 & 0 & 0 & 0 \\ 0 & 0 & 0 & 0 & 0 & 0 \\ K_{idp2}K_{vdi} & 0 & 0 & 0 & 0 & 0 \\ 0 & K_{iqp2}K_{vqi} & 0 & 0 & 0 & 0 \end{bmatrix} \\
 D &= \begin{bmatrix} K_{idp1}K_{vdi} & 0 & K_{idi1} & 0 & 0 & 0 \\ 0 & K_{iqp1}K_{vqi} & 0 & K_{iqi1} & 0 & 0 \\ 0 & 0 & 0 & 0 & K_{idi2} & 0 \\ 0 & 0 & 0 & 0 & 0 & K_{iqi2} \end{bmatrix} \\
 F &= \begin{bmatrix} 0 & 0 & 0 & 0 & 0 & 0 \\ 0 & 0 & 0 & 0 & 0 & 0 \\ K_{vdi} & 0 & 0 & 0 & 0 & 0 \\ 0 & K_{vqi} & 0 & 0 & 0 & 0 \\ 0 & 0 & 0 & 0 & 0 & 0 \\ 0 & 0 & 0 & 0 & 0 & 0 \end{bmatrix} \\
 F_d &= \begin{bmatrix} 0 & 0 & 0 & 0 & 0 & 0 \\ 0 & 0 & 0 & 0 & 0 & 0 \\ 0 & 0 & 0 & 0 & 0 & 0 \\ 0 & 0 & 0 & 0 & 0 & 0 \\ K_{vdi} & 0 & 0 & 0 & 0 & 0 \\ 0 & K_{vqi} & 0 & 0 & 0 & 0 \end{bmatrix} \\
 C &= \begin{bmatrix} 0 & 0 & 0 & 0 & 0 & 0 & -K_{idp1}K_{vdp} & 0 & -K_{idp1} & 0 & 0 & 0 \\ 0 & 0 & 0 & 0 & 0 & 0 & 0 & -K_{iqp1}K_{vqp} & 0 & -K_{iqp1} & 0 & 0 \\ 0 & 0 & 0 & 0 & 0 & 0 & 0 & 0 & 0 & 0 & -K_{idp2} & 0 \\ 0 & 0 & 0 & 0 & 0 & 0 & 0 & 0 & 0 & 0 & 0 & -K_{iqp2} \end{bmatrix} \\
 B_w &= \begin{bmatrix} 0 & 0 & \frac{1}{L_1} & \frac{1}{L_1} & 0 & 0 & 0 & 0 & 0 & 0 & 0 & 0 & 0 & 0 & 0 & 0 & 0 \\ 0 & 0 & 0 & 0 & \frac{1}{L_2} & \frac{1}{L_2} & 0 & 0 & 0 & 0 & 0 & 0 & 0 & 0 & 0 & 0 & 0 \end{bmatrix}^T \\
 B_d &= \begin{bmatrix} B_w \\ 0 \end{bmatrix}^T
 \end{aligned}$$

The uncertainty,  $w(t)$ , represents the fluctuation caused by the PV and wind energy sources;  $K_{vdp}$ ,  $K_{vqp}$ ,  $K_{vdi}$ , and  $K_{vqi}$  are the PI controller gains of the voltage control loop;  $K_{idp1}$ ,  $K_{iqp1}$ ,  $K_{idi1}$ , and  $K_{iqi1}$  are the PI controller gains of the master current controller;  $K_{idp2}$ ,  $K_{iqp2}$ ,  $K_{idi2}$ , and  $K_{iqi2}$  are the PI controller gains of the slave current controller.  $\Phi_d$ ,  $\Phi_q$  are the integrals of master voltage controller;  $\gamma_1$ ,  $\gamma_2$ , are the integrals of master current controller;  $\gamma_3$  and  $\gamma_4$  are the integrals of slave current controller. Substituting (13) into (1) and rewriting the equations in compact matrix form along with (11), [4], we get:

$$\begin{bmatrix} \dot{x}(t) \\ \dot{z}(t) \end{bmatrix} = \begin{bmatrix} A + BC & BD \\ E & F \end{bmatrix} \begin{bmatrix} x(t) \\ z(t) \end{bmatrix} + \begin{bmatrix} BC_d & BD_d \\ E_d & F_d \end{bmatrix} \begin{bmatrix} x(t - \tau(t)) \\ z(t - \tau(t)) \end{bmatrix} + \begin{bmatrix} B_w \\ 0 \end{bmatrix} w(t) \tag{14}$$

Equation (14) can be rewritten in a concise matrix form [4]:

$$\dot{x}_{cl}(t) = A_0x_{cl}(t) + A_dx_{cl}(t - \tau(t)) + B_w w(t) \tag{15}$$

$$x(t) = \Phi(t) \quad t \in [-\rho, 0] \tag{16}$$

$\Phi(t)$  is defined as the initial condition over the interval  $t \in [-\rho, 0]$ . The time delay should satisfy the following condition:

$$0 \leq \tau(t) \leq \rho, \quad \dot{\tau}(t) \leq \mu \leq 1 \tag{17}$$

The rate of the time delay change is limited by  $\mu$ , the maximum time delay should be less than  $\rho$ .

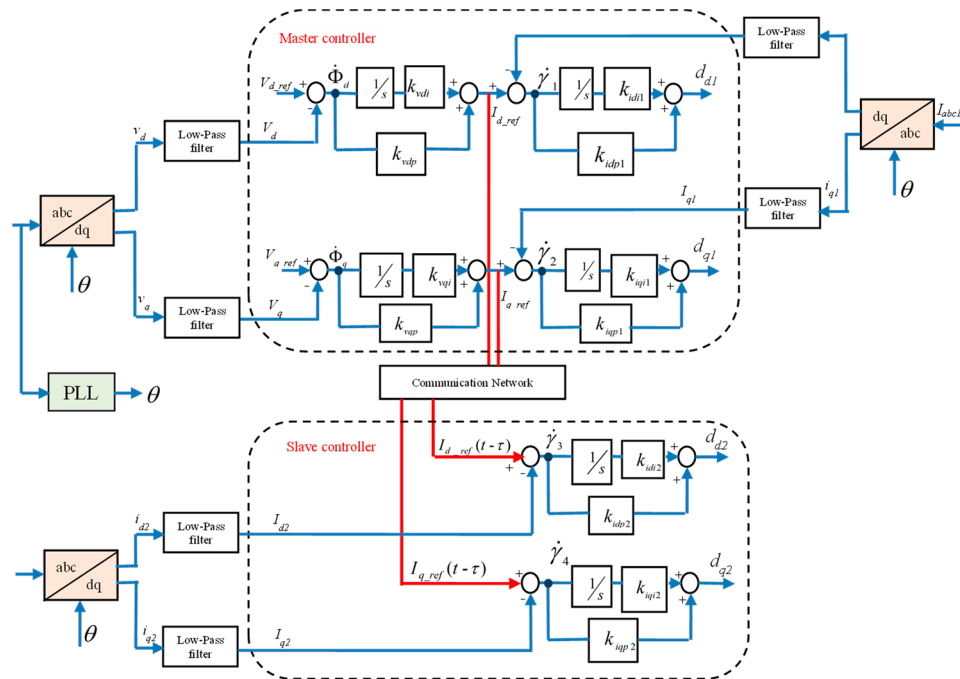


Figure 3. The controller of the master and the slave inverters.

#### 4. Robust Stability Controller Design

The robust controller synthesis for time delay system has attracted many researchers and there are different methods that can guarantee stability with time delay and uncertainties. In this paper, Lyapunov–Krasovskii functional is used to establish a stability criterion in the form of bilinear matrix inequalities. It should be noted that this approach can handle both constant and time-varying delay systems.

**Theorem 1** ([45]). *Given scalars  $\rho > 0$  and  $\mu > 0$ , the time-delay system (15) with  $w(t) = 0$  is asymptotically stable if there exist symmetric positive-definite matrices  $P = P^T > 0$ ,  $Q = Q^T > 0$  and  $Z = Z^T > 0$ , asymmetric semi-positive-definite matrix  $X = \begin{bmatrix} X_{11} & X_{12} \\ X_{12}^T & X_{22} \end{bmatrix} \geq 0$ , and any appropriate dimensioned matrices  $Y$  and  $T$  such that the following LMIs are true:*

$$\Phi = \begin{bmatrix} \Phi_{11} & \Phi_{12} & \rho A^T Z \\ \Phi_{12}^T & \Phi_{22} & \rho A_d^T Z \\ \rho Z A & \rho Z A_d & -\rho Z \end{bmatrix} < 0 \quad \Psi = \begin{bmatrix} X_{11} & X_{12} & Y \\ X_{12}^T & X_{22} & T \\ Y^T & T^T & Z \end{bmatrix} \geq 0$$

where

$$\begin{aligned} \Phi_{11} &= PA + A^T P + Y + Y^T + Q + \rho X_{11} \\ \Phi_{12} &= PA_d - Y + T^T + \rho X_{12} \\ \Phi_{22} &= -T - T^T - (1 - \mu)Q + \rho X_{22} \end{aligned}$$

Theorem 1 can be used to design a stabilizing controller for the Microgrid with variable time delay but with a deterministic system model. For given controller parameters, the delay margin can be computed, and for a given time delay the controller can be derived.

To derive a stability criterion, we choose LKF candidate as follows:

$$V(t) = x^T(t)Px(t) + \int_{t-\tau}^t x^T(s)Qx(s)ds + h \int_{-\tau}^0 \int_{t-\theta}^t \dot{x}^T(s)R\dot{x}(s)dsd\theta \tag{18}$$

$P > 0, Q > 0, R > 0$ , and  $V(t) > 0$ .

Applying LKF for system (15):

$$\begin{aligned} \dot{V}(t) = & x^T(t)P\dot{x}(t) + \dot{x}^T(t)Px(t) + x^T(t)Qx(t) - x^T(t-\tau)Qx(t-\tau) \\ & + \tau^2\dot{x}^T(t)R\dot{x}(t) - \tau \int_{t-\tau}^t \dot{x}^T(s)R\dot{x}(s)ds \end{aligned} \tag{19}$$

To simplify (19) Jensen Integral Inequality can be used, where it is defined as [45]:

Let  $f$  be an integrable function defined on  $[a, b]$  and let  $\varphi$  be a continuous (this is not needed) convex function defined at least on the set  $[m, M]$  where  $m$  is the int of  $f$  and  $M$  is the sup of  $f$ . Then

$$\varphi\left(\frac{1}{b-a} \int_a^b f\right) \leq \frac{1}{b-a} \varphi(f)$$

Applying Jensen Integral Inequality to (19) yields:

$$\begin{aligned} \dot{V}(t) = & 2x^T(t)P\dot{x}(t) + x^T(t)Qx(t) - x^T(t-T)Qx(t-T) + \\ & \tau^2x^T(t)R\dot{x}(t) - (x(t) - x(t-\tau))^T R(x(t) - x(t-\tau)) \end{aligned} \tag{20}$$

$$\begin{aligned} \dot{V} = & 2x^T(t)P[Ax(t) + A_d x(t-\tau) + B_\omega \omega(t)] + x^T(t)Qx(t-\tau) + \tau^2x^T(t)R[Ax(t) + \\ & A_d x(t-\tau) + B_\omega \omega(t)] - (x(t) - x(t-\tau))^T R(x(t) - x(t-T)) \end{aligned} \tag{21}$$

$$\begin{aligned} \dot{V}(x(t)) = & 2x^T(t)PAx(t) + 2x^T(t)PA_d x(t-\tau) + 2x^T(t)PB_\omega \omega(t) + x^T(t)Qx(t-\tau) + \tau^2x^T(t)RAx(t) \\ & + \tau^2x^T(t)RA_d x(t-\tau) + \tau^2x^T(t)RB_\omega \omega(t) - x(t) + x(t-\tau)^T Rx(t) - x(t-\tau)^T Rx(t-\tau) \end{aligned} \tag{22}$$

The necessary and sufficient condition for the stability of the system with specific  $H_\infty$  performance index requires that  $\dot{V}(x(t)) < 0$ . The system is stable with  $\gamma$  as performance as defined below.

Definition of  $H_\infty$ :

The  $H_\infty$  performance index,  $\gamma$  is a function of which  $\frac{\|z(t)\|}{\|\omega(t)\|} \leq \gamma$

$$\int_0^\infty [z^T(s)z(s) - \gamma^2 \omega^T(s)\omega(s)] ds \leq 0 \tag{23}$$

Augmenting  $x(t)$ ,  $x(t-\tau)$  and  $\omega(t)$  in one vector, that is

$$\zeta(t) = [x(t), x(t-\tau), \omega(t)] \tag{24}$$

Applying,  $\dot{V}(t) + z^T(t)z(t) - \gamma^2 \omega^T(t)\omega(t) < \zeta^T(t)\phi\zeta(t)$

Then the system is stable if:

$$P > 0, Q > 0, R > 0$$

and

$$\varphi = E_1^T P E_s + E_s^T P E_1 + E_1^T (Q + C_z^T C_z) E_1 - E_2^T Q E_2 + h^2 E_s^T R E_s - \gamma^2 E_3^T E_3 - (E_1 - E_2)^T R (E_1 - E_2) < 0 \tag{25}$$

where  $E_s = [A, A_d, B_\omega]$ ,  $E_1 = [I, 0, 0]$ ,  $E_2 = [0, I, 0]$  and  $E_3 = [0, 0, I]$ .

This can be summarized in Theorem 2.

**Theorem 2.** For a given delay  $\tau$ , the  $H_\infty$  robust performance index  $\gamma$ , the closed-loop system (15) is stable and has performance index  $\gamma$  against a non-zero disturbance for any delays smaller than  $\tau$  if there exist symmetric matrices  $P > 0$ ,  $Q > 0$ , and  $R > 0$ , such that the following linear matrix inequality hold.

$$\varphi = E_1^T P E_s + E_s^T P E_1 + E_1^T (Q + C_z^T C_z) E_1 - E_2^T Q E_2 + h^2 E_s^T R E_s - \gamma^2 E_3^T E_3 - (E_1 - E_2)^T R (E_1 - E_2) < 0$$

Equation (25) is a bilinear matrix inequality and the solution cannot be straightforward. The controller gains are the elements of matrix  $A_d$  which is a submatrix in  $E_s$ . The matrix  $E_s$  contains our controller variables and it is multiplied by  $P$ , which is also a variable matrix. The optimization problem is formulated as:

Minimize:

$$\gamma = f\left(\tau, K_{vdp}, K_{vqp}, K_{vdi}, K_{vqi}, K_{idp1}, K_{iqp1}, K_{idi1}, K_{iqi1}, K_{idp2}, K_{iqp2}, K_{idi2}, K_{iqi2}\right)$$

Subject to:

$$\begin{aligned} 0.1 < K_{vdp} < 20 \quad 0.1 < K_{vqp} < 20 \\ 50 < K_{vdi} < 1000 \quad 50 < K_{vqi} < 1000 \\ 0.1 < K_{idp1} < 4 \quad 10 < K_{iqp1} < 200 \\ 10 < K_{idi1} < 200 \quad 10 < K_{iqi1} < 200 \\ 0.1 < K_{idp2} < 4 \quad 10 < K_{iqp2} < 200 \\ 10 < K_{idi2} < 200 \quad 10 < K_{iqi2} < 200 \end{aligned}$$

When the control gains are fixed, the BMI in (25) becomes LMI in  $Q, P, R$ , and  $\gamma$ . The LMIs are then solved using Matlab. Several algorithms can be used to achieve a solution to the optimization problem, GWO is used in this paper. The GWO is introduced by [46]. Grey wolves follow a very specific dominant hierarchy in their hunting to determine the task of each group in the grey wolf hierarchy. At the top of the table are the alphas, which are the leaders of the entire pack. The main role of an alpha is to make the final decisions in hunting. Following the alpha is called the beta (second level). The role of the beta is to assist the alpha and command the rest of the wolves. The beta acts as a link between the alpha and the lower levels wolves, it supports the commands from alpha and passes them to the pack. Meanwhile, the beta passes feedback from the lower levels to the alpha. While the lowest level is the omega, their role is basically to do tasks that are given by their alpha or beta. There is one more rank between the beta and the omega, that is the delta. They are the scouts, hunters, and caretakers. The roles of delta are to watch the boundaries of the territory and warn the pack if there is any danger.

In mathematical language, the alpha is the fittest solution, the second and the third solutions are the beta and delta respectively. While the omega represents other possible candidate solutions. Grey wolves search for their prey by spreading out their position, the first diverge from each other. Eventually, they will converge back to one specific position leading them to their prey. In this case, the fittest solution. The GWO algorithm is applied in three steps: encircling, hunting, and attacking.

Encircling: When the prey is located, the grey wolves surround it.

$$D_p = |C \cdot X_p(k) - X(k)| \tag{26}$$

$$X(k+1) = X_p(k) - A \cdot D_p \tag{27}$$

where  $k$  is the number of iterations,  $X(k)$  represents the current grey wolf position,  $X(k+1)$  is the future position of the wolf,  $X_p(k)$  refers to either  $\alpha, \beta, \delta$ ,  $A$ , and  $C$  are coefficients and given as follows.

$$A = 2ar_1 - a \tag{28}$$

$$C = 2r_2 \tag{29}$$

where  $r_1, r_2$  are random vectors in the range  $[0, 1]$ , and  $a$  is in the range  $[0, 2]$ . Hunting: the pack hunts the prey, under the leadership of  $\alpha, \beta, \delta$ . This process is expressed as:

$$\begin{aligned} D_\alpha &= |C_1 \cdot X_\alpha - X(k)| \\ D_\beta &= |C_2 \cdot X_\beta - X(k)| \end{aligned} \tag{30}$$

$$\begin{aligned} D_\delta &= |C_3 \cdot X_\delta - X(k)| \\ X_1 &= X_\alpha(k) - A_1 D_\alpha \\ X_2 &= X_\beta(k) - A_2 D_\beta \end{aligned} \tag{31}$$

$$X_3 = X_\delta(k) - A_3 D_\delta \tag{32}$$

Attacking: Grey wolves encircled the prey and start to be ready to seize the prey (numerical convergence), because of  $A \in [-2a, 2a]$ . The attack stage is achieved by the decrement of  $a$  in (28). When  $|A| \geq 1$ , the search is still global and grey wolves will be far away from the prey; when  $|A| < 1$ , the grey wolves are close to the prey and ready to attack. This sums up the algorithm for the GWO. In summary, the hunting process of grey wolves to be implemented in this research is first to define the number of grey wolves (number of solutions) in the GWO algorithm. With a few iterations, the alpha, beta, and delta determine the possible solution. The parameter  $a$  is decreased from 2 to 0 for further exploration and exploitation. When  $|\vec{A}| > 1$ , the candidate solution diverges from the optimum solution and converges toward the optimum solution when  $|\vec{A}| < 1$ . When the criterion is satisfied, the GWO algorithm is terminated as shown in Figure 4.

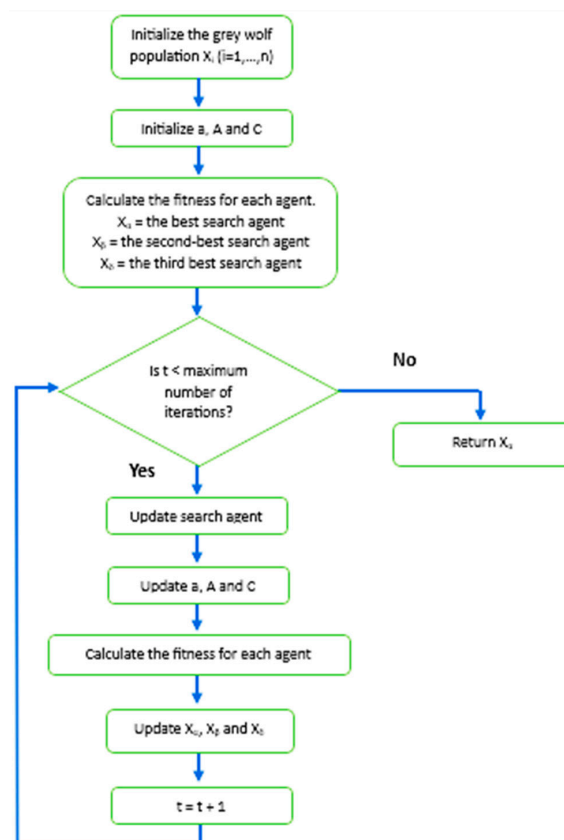


Figure 4. The GWO algorithm.

### 5. Results

The results in this paper are generated using Matlab/Simulink. In this simulation, the system frequency is 50 Hz, the components of the filter in the two-parallel inverter are  $C = 22 \mu F$  and  $L_1 = L + L_2 = 4 mH$ , and  $R = 4.25 \Omega$ . In [47], the controller gains which achieve good performance are obtained using classical tuning techniques. Solving the BMI in Theorem 2, the system is robust stable with  $\gamma = 0.238$ , the controller gains are:  $K_{vdp} = 18.1253$ ,  $K_{vqp} = 12.6839$ ,  $K_{vdi} = 569.5374$ ,  $K_{vqi} = 199.7324$ ,  $K_{idp1} = 1.9930$ ,  $K_{idp2} = 1.7449$ ,  $K_{idi1} = 192.3036$ ,  $K_{idi2} = 171.3346$ ,  $K_{iqp1} = 153.9706$ ,  $K_{iqp2} = 134.5408$ ,  $K_{iqi1} = 16.0482$ ,  $K_{iqi2} = 28.4550$ . The preexist time delay is set to 0.61 ms. For the GWO the SearchAgents\_no = 3, and the Max\_iteration = 3.

The PV array produces 45 A at 400 V, which makes the output power 18 kW. The rectifier produces 45.122 A at 410 V which makes the output power of the wind energy conversion system around 18.5 kW. To test the controller under transient and steady state, the simulation was started with zero initial conditions. The transient takes around 10 ms. The DC currents and voltages of the PV system and wind energy conversion system are shown in Figures 5 and 6.

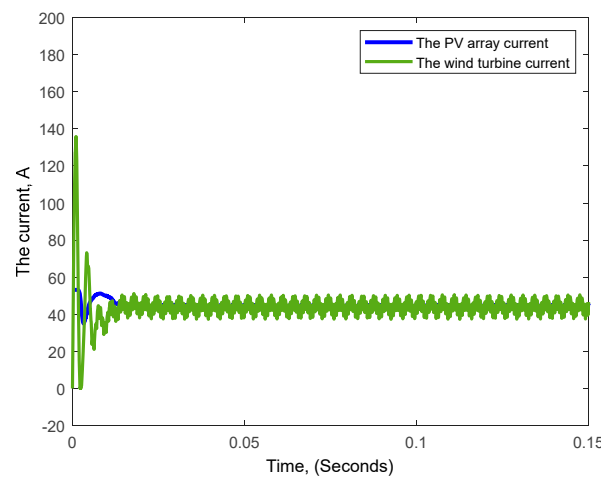


Figure 5. The DC input currents of the inverters.

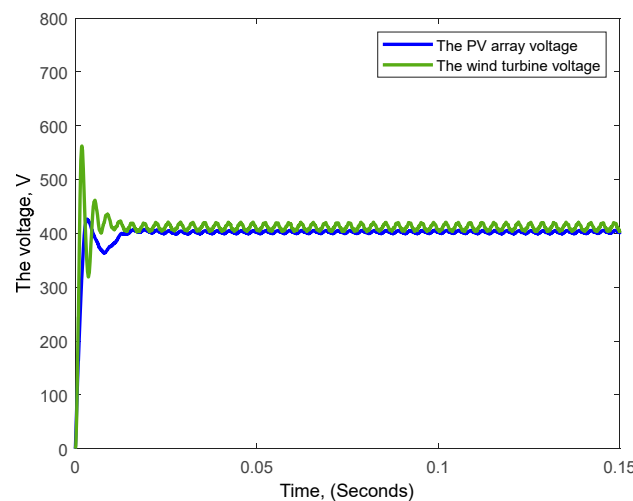


Figure 6. The DC input voltage of the inverters.

The terminal voltages of the microgrid show a stable operation and regulated voltages as can be seen from Figure 7. The two inverters produce equal three-phase currents as shown in Figure 8, and it clearly shows that the current is evenly distributed. The two inverters produce three-phase current of around 108 A as shown in Figure 9. The synchronization is carried out through PLL, and Figure 10 shows the single-phase currents

of the first and the second inverter. Taking a smaller time scale (0.015 s), it is clear that the two inverters are synchronized, and we notice only small deviation during the transient condition.

The real and reactive powers of both inverters are shown in Figure 11. The two renewable energy sources transfer their maximum produced power and supply it to the load. It should be noted that the first inverter produces the reactive power while the second inverter absorbs it. As the time delay is time varying and in most of the cases obtaining accurate model is not possible, so in this paper, the stability of the system was carried out based on Lyapunov–Krasovskii functional and  $H_\infty$  robustness performance index. Another important approach is to determine the maximum delay margin of the system based on the analysis in s-domain. Based on our knowledge, this is the first time the GWO is used to design a robust controller for networked microgrid with variable time delay and uncertainties. The Speedgoat hardware-in-the-loop real-time and practical set-up will be developed to test the proposed approach.

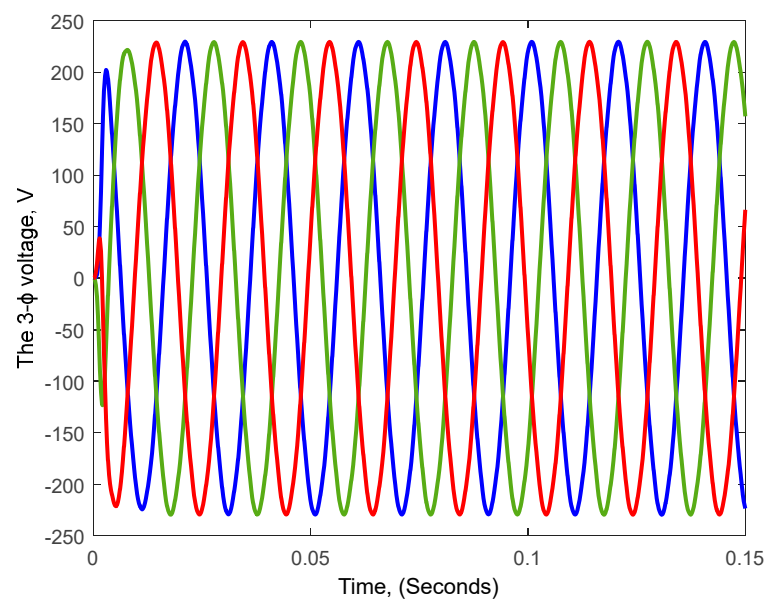


Figure 7. The three-phase output voltages.

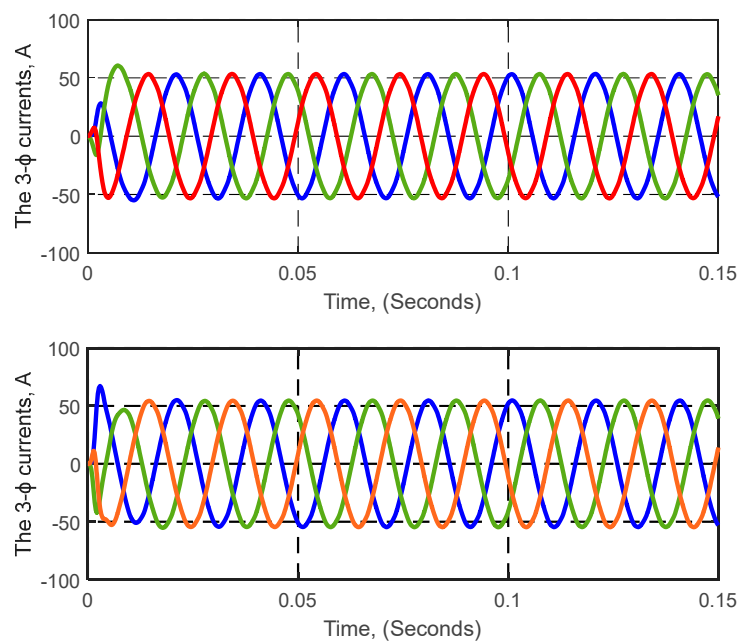


Figure 8. The output currents of both inverters.

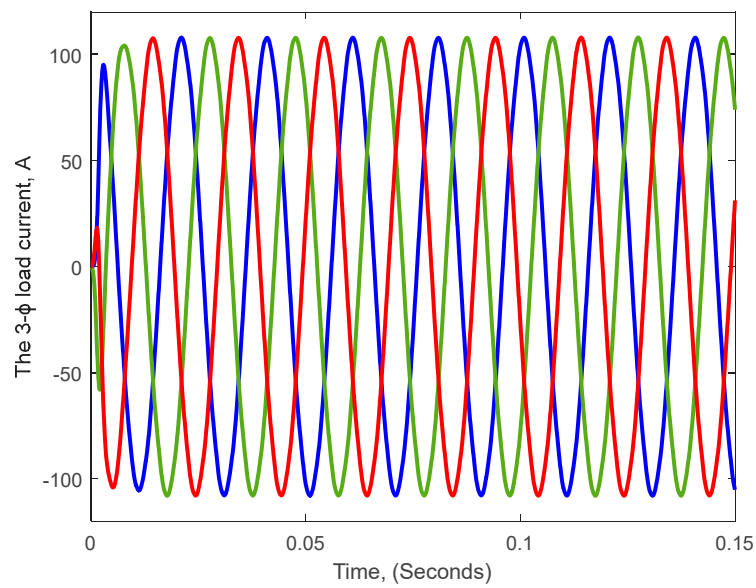


Figure 9. The output load currents.

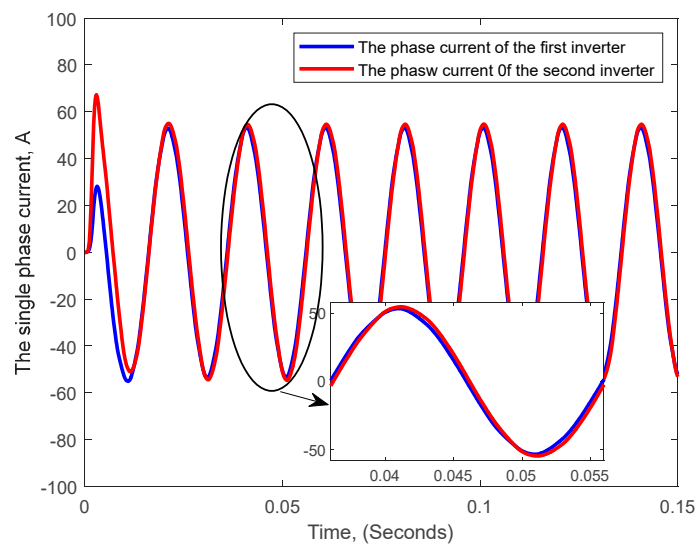


Figure 10. Synchronized phase currents of both inverters.

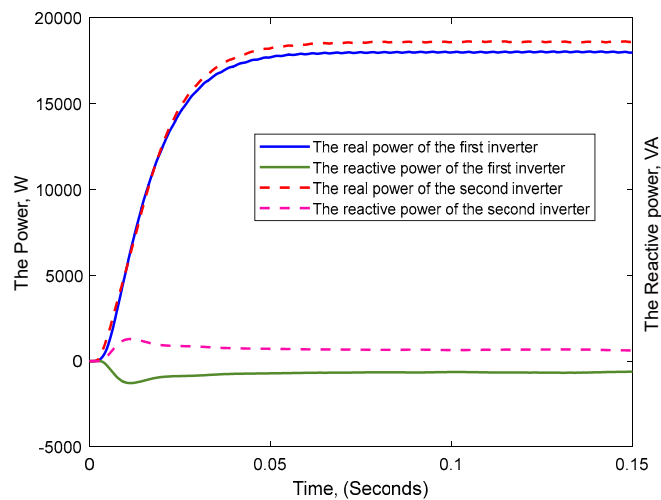


Figure 11. The active and reactive power of both inverters.

## 6. Conclusions

In this paper the robust stability of microgrid with time delay and uncertainty in renewable energy sources is investigated. The master-slave control is implemented, where the time delay exists in the closed-loop control system. Additionally, the time-varying nature of the renewable energy sources could lead to instability. Lyapunov–Krasovskii function and robust  $H_\infty$  stability theorem are used to develop stability criterion. The controller design problem is formulated as bilinear matrix inequality. The grey wolf optimization is used to solve the bilinear matrix inequality and to derive the stabilizing controller that guarantees specific RPI. The proposed control design procedure has been applied to a two-inverters microgrid and the performance is validated using the nonlinear models of the microgrid. The performance of the microgrid is accepted even with the presence of the time delay and uncertainty in renewable energy sources. Additionally, power sharing is achieved with no significant distortion.

**Author Contributions:** Conceptualization, A.K. (Ashraf Khalil) and A.K. (Asma Alfergani); methodology, A.K. (Asma Alfergani); writing—original draft preparation, A.K. (Ashraf Khalil), A.K. (Asma Alfergani), F.M.S. and A.A.; writing—review and editing, A.K. (Ashraf Khalil), A.K. (Asma Alfergani), F.M.S. and A.A. All authors have read and agreed to the published version of the manuscript.

**Funding:** This research received no external funding.

**Informed Consent Statement:** Not applicable.

**Acknowledgments:** This manuscript was supported financially by DTU. The authors would like to use this opportunity to thank DTU.

**Conflicts of Interest:** The authors declare no conflict of interest.

## References

1. Prodanovic, M.; Green, T.C.; Mansir, H. A survey of control methods for three-phase inverters in parallel connection. In Proceedings of the 2000 Eighth International Conference on Power Electronics and Variable Speed Drives, London, UK, 18–19 September 2000; pp. 472–477. [\[CrossRef\]](#)
2. Alfergani, A.; Alfajori, K.A.; Khalil, A.; Buaozza, N. Control strategies in AC microgrid: A brief review. In Proceedings of the 2018 9th International Renewable Energy Congress (IREC), Hammamet, Tunisia, 20–22 March 2018; pp. 1–6.
3. Kaviri, S.M.; Pahlevani, M.; Jain, P.; Bakhshai, A. A review of AC microgrid control methods. In Proceedings of the 2017 IEEE 8th International Symposium on Power Electronics for Distributed Generation Systems (PEDG), Florianopolis, Brazil, 17–20 April 2017; pp. 1–8. [\[CrossRef\]](#)
4. Alfergani, A.; Khalil, A.; Rajab, Z. Networked control of AC microgrid. *Sustain. Cities Soc.* **2018**, *37*, 371–387. [\[CrossRef\]](#)
5. Rajab, Z.; Sassi, Y.; Taher, A.; Khalil, A.; Mohamed, F. A practical seasonal performance evaluation of small wind turbine in urban environment. *Wind. Eng.* **2019**, *43*, 344–358. [\[CrossRef\]](#)
6. Margoum, E.; Krami, N. Design and control strategy of micro-wind turbine based PMSM in AC MicroGrid. In Proceedings of the 2016 17th International Conference on Sciences and Techniques of Automatic Control and Computer Engineering (STA), Sousse, Tunisia, 19–21 December 2016; pp. 575–581.
7. Khalil, A.; Ateea, K. Modelling and control of photovoltaic-based microgrid. *Int. J. Renew. Energy Res.* **2015**, *5*, 826–835.
8. Khalil, A.; Alfajori, K.A.; Elbarsha, A. Stability analysis of parallel-inverters in microgrid. In Proceedings of the 2014 20th International Conference on Automation and Computing, Bedfordshire, UK, 12–13 September 2014; pp. 110–115.
9. Alfergani, A.; Khalil, A. Modeling and control of master-slave microgrid with communication delay. In Proceedings of the 2017 8th International Renewable Energy Congress (IREC), Amman, Jordan, 21–23 March 2017; pp. 1–6.
10. Khalil, A.; Alfajori, K.A.; Asheibi, A. Modeling and control of PV/Wind Microgrid. In Proceedings of the 2016 7th International Renewable Energy Congress (IREC), Hammamet, Tunisia, 22–24 March 2016; pp. 1–6.
11. Lai, J.; Lu, X.; Wang, F.; Dehghanian, P.; Tang, R. Broadcast gossip algorithms for distributed peer-to-peer control in ac microgrids. *IEEE Trans. Ind. Appl.* **2019**, *55*, 2241–2251. [\[CrossRef\]](#)
12. Dou, C.; Yue, D.; Zhang, Z.; Ma, K. MAS-based distributed cooperative control for DC microgrid through switching topology communication network with time-varying delays. *IEEE Syst. J.* **2017**, *13*, 615–624. [\[CrossRef\]](#)
13. Lai, J.; Lu, X.; Yu, X.; Monti, A.; Zhou, H. Distributed voltage regulation for cyber-physical microgrids with coupling delays and slow switching topologies. *IEEE Trans. Syst. Man Cybern. Syst.* **2019**, *50*, 100–110. [\[CrossRef\]](#)
14. Zhang, Z.; Dou, C.; Yue, D.; Zhang, B.; Zhang, T. Photovoltaic voltage regulation through distributed power compensation considering communication delay. *Adv. Theory Simul.* **2020**, *3*, 1900148. [\[CrossRef\]](#)

15. Xu, S.; Sun, H.; Zhang, Z.; Guo, Q.; Zhao, B.; Bi, J.; Zhang, B. MAS-Based Decentralized Coordinated Control Strategy in a Micro-Grid with Multiple Microsources. *Energies* **2020**, *13*, 2141. [[CrossRef](#)]
16. Yan, H.; Zhou, X.; Zhang, H.; Yang, F.; Wu, Z.-G. A novel sliding mode estimation for microgrid control with communication time delays. *IEEE Trans. Smart Grid* **2017**, *10*, 1509–1520. [[CrossRef](#)]
17. Shrivastava, S.; Subudhi, B.; Das, S. Communication Delay Analysis of Consensus-based Secondary Control of Islanded Microgrid. In Proceedings of the 2018 15th IEEE India Council International Conference (INDICON), Coimbatore, India, 16–18 December 2018; pp. 1–6.
18. Lai, J.; Lu, X.; Yu, X.; Yao, W.; Wen, J.; Cheng, S. Distributed multi-DER cooperative control for master-slave-organized microgrid networks with limited communication bandwidth. *IEEE Trans. Ind. Inform.* **2018**, *15*, 3443–3456. [[CrossRef](#)]
19. Zhang, B.; Zhang, Z.; Liu, L.; Luo, W.; Wu, D.; Dou, C. A Novel Consensus-based Secondary Control Strategy for Isolated Microgrid Facing with Communication Interruption. In Proceedings of the 2018 5th IEEE International Conference on Cloud Computing and Intelligence Systems (CCIS), Nanjing, China, 23–25 November 2018; pp. 1023–1027.
20. Xie, Y.; Lin, Z. Distributed event-triggered secondary voltage control for microgrids with time delay. *IEEE Trans. Syst. Man Cybern. Syst.* **2019**, *49*, 1582–1591. [[CrossRef](#)]
21. Zhijie, L.; Deng, C.; Wen, C.; Guo, F.; Lin, P.; Jiang, W. Distributed Event-Triggered Control for Frequency Restoration and Active Power Allocation in Microgrids with Varying Communication Time Delays. *IEEE Trans. Ind. Electron.* **2020**, *68*, 8367–8378.
22. Shi, M.; Chen, X.; Zhou, J.; Chen, Y.; Wen, J. Frequency Restoration and Oscillation Damping of Distributed VSGs in Microgrid with Low Bandwidth Communication. *IEEE Trans. Smart Grid* **2020**, *12*, 1011–1021. [[CrossRef](#)]
23. Cady, S.T.; Zholbaryssov, M.; Domínguez-García, A.D.; Hadjicostis, C.N. A distributed frequency regulation architecture for islanded inertialess ac microgrids. *IEEE Trans. Control. Syst. Technol.* **2017**, *25*, 1961–1977. [[CrossRef](#)]
24. Simpson-Porco, J.W.; Shafiee, Q.; Dörfler, F.; Vasquez, J.C.; Guerrero, J.M.; Bullo, F. Secondary frequency and voltage control of islanded microgrids via distributed averaging. *IEEE Trans. Ind. Electron.* **2015**, *62*, 7025–7038. [[CrossRef](#)]
25. Li, Z.; Zang, C.; Zeng, P.; Yu, H.; Li, S.; Bian, J. Control of a Grid-Forming Inverter Based on Sliding-Mode and Mixed  $H_2/H_\infty$  Control. *IEEE Trans. Ind. Electron.* **2016**, *64*, 3862–3872. [[CrossRef](#)]
26. Dou, C.; Yue, D.; Guerrero, J.M.; Xie, X.; Hu, S. Multiagent system-based distributed coordinated control for radial DC microgrid considering transmission time delays. *IEEE Trans. Smart Grid* **2016**, *8*, 2370–2381. [[CrossRef](#)]
27. Bevrani, H.; Feizi, M.R.; Ataee, S. Robust Frequency Control in an Islanded Microgrid:  $H_\infty$  and  $\mu$ -Synthesis Approaches. *IEEE Trans. Smart Grid* **2015**, *7*, 706–717. [[CrossRef](#)]
28. Dou, C.; Yue, D.; Zhang, Z.; Guerrero, J.M. Hierarchical delay-dependent distributed coordinated control for DC ring-bus microgrids. *IEEE Access* **2017**, *5*, 10130–10140. [[CrossRef](#)]
29. Kerdphol, T.; Rahman, F.S.; Watanabe, M.; Mitani, Y. Robust virtual inertia control of a low inertia microgrid considering frequency measurement effects. *IEEE Access* **2019**, *7*, 57550–57560. [[CrossRef](#)]
30. Ali, H.; Magdy, G.; Li, B.; Shabib, G.; Elbaset, A.A.; Xu, D.; Mitani, Y. A new frequency control strategy in an islanded microgrid using virtual inertia control-based coefficient diagram method. *IEEE Access* **2019**, *7*, 16979–16990. [[CrossRef](#)]
31. Raeispour, M.; Atrianfar, H.; Baghaee, H.R.; Gharehpetian, G.B. Resilient  $H_\infty$  Consensus-based Control of Autonomous AC Microgrids with Uncertain Time-Delayed Communications. *IEEE Trans. Smart Grid* **2020**, *11*, 3871–3884. [[CrossRef](#)]
32. Mahmoud, M.S.; Alyazidi, N.M. Quantized  $H_\infty$  Estimator Over Communication Networks for Distributed Generation Units. *IEEE Trans. Syst. Man, Cybern. Syst.* **2017**, *50*, 1134–1146. [[CrossRef](#)]
33. Wang, T.; Gao, H.; Qiu, J. A combined adaptive neural network and nonlinear model predictive control for multirate networked industrial process control. *IEEE Trans. Neural Netw. Learn. Syst.* **2015**, *27*, 416–425. [[CrossRef](#)] [[PubMed](#)]
34. Dinh, T.Q.; Ahn, K.K.; Marco, J. A novel robust predictive control system over imperfect networks. *IEEE Trans. Ind. Electron.* **2016**, *64*, 1751–1761. [[CrossRef](#)]
35. Wu, B.-F.; Lin, C.-H. Adaptive Neural Predictive Control for Permanent Magnet Synchronous Motor Systems with Long Delay Time. *IEEE Access* **2019**, *7*, 108061–108069. [[CrossRef](#)]
36. Tian, Y.-P.; Chun, S.; Chen, G.; Zong, S.; Huang, Y.; Wang, B. Delay Compensation-Based Time Synchronization Under Random Delays: Algorithm and Experiment. *IEEE Trans. Control. Syst. Technol.* **2021**, *29*, 80–95. [[CrossRef](#)]
37. Chen, J.; Chen, B.; Zeng, Z. Synchronization in Multiple Neural Networks with Delay via Impulsive Control with Event-Triggered Strategy and Disconnected Switching Topology. *IEEE Trans. Ind. Electron.* **2021**, *68*, 2491–2500. [[CrossRef](#)]
38. Qin, J.; Li, F.; Mou, S.; Kang, Y. Multi-timer based event synchronization control for sensor networks and its application. *IEEE Trans. Ind. Electron.* **2016**, *63*, 7765–7775. [[CrossRef](#)]
39. Li, N.; Sun, H.; Li, Z.; Zhang, Q. Adaptive semi-periodically intermittent and lag synchronization control of neural networks with mixed delays. *IEEE Access* **2017**, *6*, 4742–4749. [[CrossRef](#)]
40. Liu, R.; Cao, X.; Liu, M. Finite-time synchronization control of spacecraft formation with network-induced communication delay. *IEEE Access* **2017**, *5*, 27242–27253. [[CrossRef](#)]
41. Zhang, C.; Wang, X.; Unar, S.; Wang, S. Aperiodically intermittent control for synchronization on the delayed bipartite networks with non-delay and delay couplings. *IEEE Access* **2018**, *6*, 50939–50949. [[CrossRef](#)]
42. Walker, G. Evaluating MPPT converter topologies using a MATLAB PV model. *J. Electr. Electron. Eng.* **2001**, *21*, 49–56.
43. Heier, S. *Grid Integration of Wind Energy: Onshore and Offshore Conversion Systems*, 3rd ed.; Wiley: New York, NY, USA, 2014.

44. Krause, P.C.; Wasynczuk, O.; Sudhoff, S.D.; Pekarek, S. *Analysis of Electric Machinery and Drive Systems*; Wiley-IEEE Press: New York, NY, USA, 2002.
45. Wu, M.; He, Y.; She, J.-H. Stability analysis. In *Robust Control of Time-Delay Systems*; Springer: Berlin, Germany, 2010.
46. Mirjalili, S.; Mirjalili, S.M.; Lewis, A. Grey wolf optimizer. *Adv. Eng. Softw.* **2014**, *69*, 46–61. [[CrossRef](#)]
47. Alfergani, A.; Khalil, A.; Rajab, Z.; Zuheir, M.; Asheibi, A.; Khan, S.; Aboadla, E.H.E.; Azna, K.A.B.; Tohtayong, M. Control of master-slave microgrid based on CAN bus. In Proceedings of the 2017 IEEE Jordan Conference on Applied Electrical Engineering and Computing Technologies (AEECT), Aqaba, Jordan, 11–13 October 2017; pp. 1–6.

**Disclaimer/Publisher’s Note:** The statements, opinions and data contained in all publications are solely those of the individual author(s) and contributor(s) and not of MDPI and/or the editor(s). MDPI and/or the editor(s) disclaim responsibility for any injury to people or property resulting from any ideas, methods, instructions or products referred to in the content.